Research Article

Production, characterization and properties of open-cell calcium phosphate foams reinforced with alumina

Fani Stergioudi[1] · Ntina Al Kagiet[1] · Dimitris Thomas Kountouras[1] · Stefanos Kouparanis[1] · Emmanuil Smyrnaios[1] · Nikolaos Michailidis[1]

Abstract

In this study, tailored made open-cell calcium phosphate foams reinforced with alumina were fabricated by employing a dissolution-sintering process, using crystalline raw cane sugar as a water-leachable material. The effect of the alumina addition in the 3D morphology and in the microstructure of the produced calcium phosphate-based foams was examined. Preliminary in vitro bio-dissolution studies were performed to obtain an initial indication for the suitability of these composite bioceramic foams as implant materials. The mechanical properties of the produced composite calcium phosphate foams were also evaluated. It was found that the addition of small amount of alumina (5 wt%) resulted in a microstructural alteration affecting both the 3D geometry of the produced bioceramic foams and the morphology of the precipitated apatite during the biodegradation tests. The addition of alumina resulted in considerable enhancement of the mechanical strength of the bioceramic foam when the porosity was above 70%. The produced calcium phosphate-based composite foams (with alumina reinforcement) are suitable for biomedical applications.

Keywords Calcium phosphate foam · Alumina · Microstructure · Mechanical properties · Biodegradation

1 Introduction

Porous hydroxyapatite (HAp) has long been acknowledged in orthopedics and dentistry as a scaffold material suitable for bone and teeth replacement. This is attributed to same chemical composition of the HAp with the calcified human tissue, thus exhibiting similar biological behavior. Nevertheless, their low mechanical strength and the slow biodegradation process constitute a deterrent for their widespread use in medical applications. Therefore, for long term applications it is imperative to improve HAp's mechanical properties and bioactivity [1].

It has recently been demonstrated that the development of nanosized structures and the addition of reinforcement phases can improve the mechanical properties of HAp samples [2–10].Several new fabrication techniques such as 3D printing [11], reaction of spherical tricalcium phosphate granules [12], gel casting [7], direct hydrothermal techniques [9] and coating techniques such as MOCVD [13] were proposed in literature for production of porous HAp.

So far, several reinforcements are used to enhance the properties of HAp such as TiO_2 [14], Al_2O_3 [14–17], high content of strontium (Sr)-incorporated calcium deficient hydroxyapatite [5], hydroxyapatite nanoparticles (HANPs) [6], MgO, ZrO_2 [10, 14], etc. Among these various additives alumina, which is a bioinert material, presents certain advantages such as excellent corrosion resistance, high wear resistance, high compressive strength and high hardness. The addition of high amount of alumina (macro-sized

✉ Fani Stergioudi, fstergio@meng.auth.gr; Ntina Al Kagiet, alkantin@meng.auth.gr; Dimitris Thomas Kountouras, kountoud@civil.auth.gr; Stefanos Kouparanis, skouparanis@meng.auth.gr; Emmanuil Smyrnaios, esmyrnai@meng.auth.gr; Nikolaos Michailidis, nmichail@eng.auth.gr | [1]Physical Metallurgy Laboratory (PML), Department of Mechanical Engineering, Aristotle University of Thessaloniki, 54124 Thessaloníki, Greece.

SN Applied Sciences (2019) 1:1346 | https://doi.org/10.1007/s42452-019-1411-6

Received: 4 July 2019 / Accepted: 1 October 2019 / Published online: 5 October 2019

or nanostructured) is well documented in literature [2–4, 14–16]. However the addition of small amount of alumina to the HAp matrix is scarcely investigated. Ayed et al. [17] have shown that the addition of 2.5 wt% alumina led to improved densification of tricalcium phosphate (TCP)–26.52 wt% fluorapatite composites. Moreover they showed that alumina reacted only when the temperature was above 1400 °C [17].

In this study the effect of small alumina addition (1 and 5 wt%) on the production process and properties of calcium phosphate -based foams is investigated. More precisely the 3D morphology and microstructural morphology of the produced composite calcium phosphate-based foams was examined. Preliminary in vitro bio-dissolution studies were performed to obtain an initial indication for the suitability of these composite bioceramic foams as implant materials. The mechanical properties of the produced composite calcium phosphate foams were also examined.

2 Materials and methods

2.1 Production method of bioceramic foams

Hydroxylapatite powder ($Ca_5HO_{13}P_3$) with a mean pore size of about 10 μm provided by Fluka Chemika, alumina (Al_2O_3) powder with a mean pore size of 110 μm supplied by Alpha Aesar and raw cane sugar, in crystalline form with a relatively even size that consisted of cube like particles with smooth surfaces were used as initial materials for the production of bioceramic foams. The the pore size of the final bioceramic foam was controlled within a desired range. For these reason the sugar powder was divided by a series of sieves into two size groups: 0.5–1.0 mm and 0.125-0.5 mm, with nominal mean sizes of 0.70 and 0.35 mm respectively.

The production process for the calcium phosphate foams consisting of four stages: mixing, compaction, dissolution and sintering. The production process is thoroughly described in [18]. In summary, the HAp and alumina powders are mixed with the sugar particles at a pre-specified weight ratio depending on the desired alumina addition and the desired final porosity of bioceramic foam. In this study addition of 1 and 5 wt% alumina was investigated.

The powder mixture was uniaxially compressed at 250 MPa. The removal of the sugar from the green compact particles was achieved by water leaching. Subsequently sintering in atmospheric conditions was performed at 1250 °C for 4 h. Details for the optimum thermal cycle used in this study so as to prevent the collapse of the macro-pore network due to sintering conditions can be found in [18].

2.2 Experimental methods used

Scanning electron microscopy (SEM) (JEOL 840A scanning electron microscope working at 20 kV) was utilised to characterize the microstructure of the produced bioceramic foam. More specifically the calcium phosphate foams were sliced by a diamond saw blade and then polished with 3 and 6 μm diamond pastes. X-Ray diffraction (XRD) (2-cycle diffractometer (Philips PW 1050) with CuKa radiation) was also used to investigate the obtained crystal structure of the bioceramic foam after the sintering process.

To evaluate the pore size distribution and quantify the pore shape morphology, image analysis was performed on 2D cross-sectional slices of the foams. At least 450 pores from each foam were studied so as to have a representative and reliable statistical analysis. A watershed algorithm was applied to convert the open pores to close ones and calculate the mean size and pore size distribution. Each pore was then replaced with the best fitting ellipse that had the same volume, orientation and centroid as the original pore. Then, the mean size and pore size distribution were calculated.

The porosity of the preform (green compact) P_{pr} can be evaluated by Eq. (1):

$$P_{pr} = 1 - \frac{\rho_{pr}}{\rho_s} \tag{1}$$

where ρ_{pr} is the calculated density of the preform by measuring the weight and dimensions of the compact and ρ_s is the theoretical density of a fully dense HAp-alumina-sugar mixture. The theoretical density of the dense mixture, ρ_s, was calculated by the rule of mixtures, according to Eq. (2):

$$\rho_s = \rho_{HAp} \cdot V_{HAp} + \rho_{sugar} \cdot V_{sugar} + \rho_{alumina} \cdot V_{alumina} \tag{2}$$

where ρ_{HAP}, $\rho_{alumiuna}$ and ρ_{sugar} are the densities of HAp, alumina and raw cane sugar respectively ($\rho_{HAp} = 3.16$ gr cm^{-3}, $\rho_{alunima} = 3.95$ gr cm^{-3} and $\rho_{Sugar} = 1.57$ gr cm^{-3}) and V_i is the volume fraction of each constituent in the initial powder mixture.

The porosity of the as-manufactured ceramic foam P_f can be estimated by Eq. (3)

$$P_f = 1 - \frac{V_s}{V_f} \tag{3}$$

where V_f is the volume of the foam and V_s is the volume of solid phases of the foam which was measured based on Archimedes principle.

The linear shrinkage effect was calculated from equation

$$S = \frac{M_p - M_a}{M_p} \tag{4}$$

where M_p and M_a correspond to the diameter or length of the foam prior and after sintering, respectively (without taking into account the porosity). A calibrated calliper was used to measure the foam's dimensions prior and after sintering.

Dissolution tests were conducted in a Tris-HCl buffer solution so as to assess the effect of alumina addition in dissolution behavior and in vitro biodegradation of the produced bioceramic foams. As a reference material a calcium phosphate foam without alumina addition, produced under the same conditions (compaction pressure, sintering thermal cycle), was used. The Tris-HCl buffer is frequently used as the immersion environment for biodegradation studies because it offers an initial indication for the suitability of the materials as biocompatible. Moreover the buffer pH can range from 7-9 which coincides with the typical pH for most physiological fluid of the human organisms [19, 20].

Tris-hydroxymethyl-aminomethane ($C_4H_{11}NO_3$), supplied by Merck company was dissolved in distilled water at a 0.05 M concertation to prepare the Tris-buffer solution. The solution was then stabilized with HCl to a pH of 7.45. Each foam specimen (of about 0.7 gr) was immersed individually in 200 ml of Tris-buffer solution using 500 ml capacity flasks. The solution was then thermostatized at 37 °C and statically conserved to different time intervals ranging from 1 to 14 days. The changes in surface morphology were examined via SEM images. Sample's weight changes and pH alteration in the buffer solution were also recorded versus time.

Uniaxial static testing was performed to evaluate the compressive strength. The crosshead speed for all samples was around 0.2 mm s^{-1} which corresponded to a strain rate of approximately 0.015 s^{-1}. Cylindrical samples were used having a diameter of about 13.5 mm and length of about 14 mm. Based on the sample dimensions the stress and strain values were deduced from the recorded force–displacement data. The maximum stress and the linear slope of the stress–strain curves were used to determine the ultimate compressive strength and Young's modulus, respectively. The nominal compressive stress (σ_c) was defined as $\sigma_c = F/AP$ where, F is the load, A is the area of the specimen and P is the porosity of the sample, while the nominal strain of the specimen was determined from the crosshead displacement of the machine per length of the specimen. A minimum of five tests was performed per testing condition to guarantee the reliability of the results.

3 Results and discussion

3.1 Characterization of the produced bioceramic foams

The influence of alumina addition to the porosity of the final bioceramic foam and the porosity of the green compact (retained after the compaction stage) is shown in Fig. 1a.

For the green compact porosity we can observe that the addition of Al_2O_3 increases the retained porosity (coming from the compaction stage of the HAp powder and sugar mixture). However this rise becomes more pronounced as the volume fraction of the sugar in the mixture is increased. It should be noted that the mechanisms causing this increase in retained porosity is the same and independent from the percentage of alumina addition since the two curves present the same slope. However, the pore size plays an important role and affects the retained porosity in the green compact. The reason of the increase of the retained porosity of green compact is attributed to the addition of hard alumina particles that are non-deformable thus prevented the compaction of the powder mixture.

HAp powder is harder and more difficult to deform than the sugar particles. Thus the low volume fraction of Hap powder leads to denser green compacts. The barrier to compaction with the addition of micro-sized alumina is ascribed to mechanical engagement phenomena and friction effects. Friction is stronger for small particle sizes because of the high surface area inhibiting thus the densification process and reducing the compressibility of the material mixture. The fact that the pore size affects the retained porosity for a given volume fraction of sugar particles enhances this presumption. When the pore size is reduced (meaning that the sugar particles are smaller) the resulting structure presents a more uniform distribution of the struts having lower thickness (see Fig. 1d). Consequently each individual strut has lower percentage of alumina particles thus enhancing the compressibility.

However the final structure and porosity of the bioceramic foam is controlled by another parameter. Shrinkage seems to be the prevailing mechanism given that in all examined cases, a linear shrinkage ranging from 12 to 18% was observed. Pore size (e.g. the size of the sugar particle) has no effect in shrinkage percentage and consequently to the final porosity of the bioceramic foam. The alumina addition has a considerable effect on the final porosity since the measured porosity of the foams approached the theoretical value of porosity (Fig. 1a). Theoretically, the porosity of the bioceramic foam is equivalent to the volume fraction of the sugar in the initial sugar/HAp mixture. This means that the addition of alumina leads to reduction of microporosity of the resultant bioceramic foam which was also confirmed by the microstructural characterization of the foam (Fig. 2). The microstructure of pure HAp-foam sintered at 1250 °C for 4 h exhibits intense surface microporosity. A rounding of particles is apparent at higher magnification images which is ascribed mainly to surface and

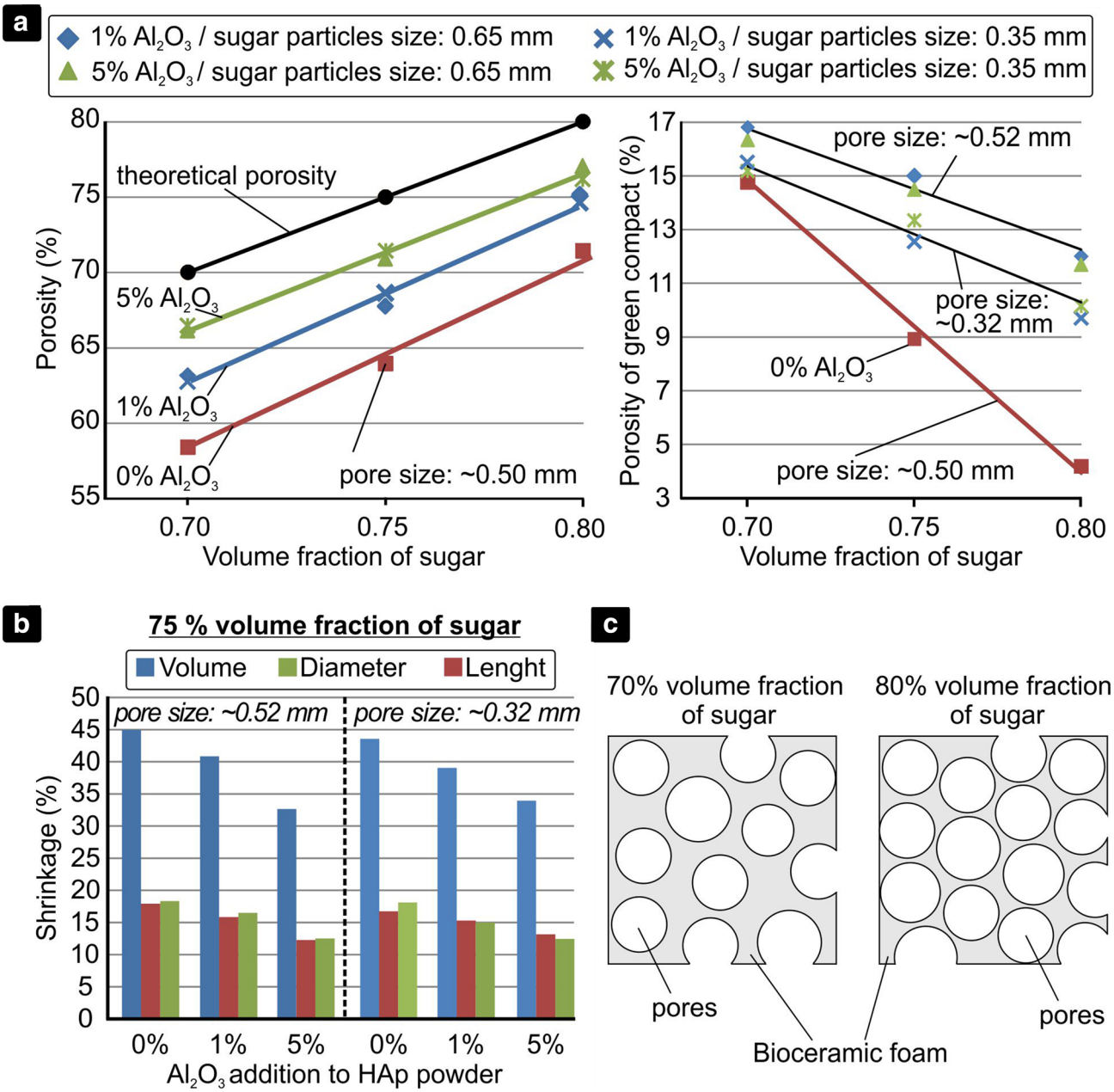

Fig. 1 **a** Variation between the actual porosity and theoretical porosity of the bioceramic foams and **b** indicative linear and volume shrinkage percentage of the bioceramic foams after sintering at 1250 °C for 4 h, **c** variation of strut thickness in the produced bioceramic foam as a function of the volume fraction of sugar powder in the initial powder mixture

volume diffusion phenomena, leading to approximately equi-axed grains.

The formation of the microporosity can be ascribed to reactions that occur during sintering. More specifically it is reported that the HAp decomposes and releases H_2O gas leading thus to formation of micropores. The probable reactions that may occur are [21, 22].

$$Ca_{10}(PO_4)_6(OH)_2 \rightarrow Ca_3(PO_4)_2 + CaO + H_2O \uparrow \quad (1)$$ and

$$Ca_{10}(PO_4)_6(OH)_2 \rightarrow Ca_3(PO_4)_2 + Ca_4P_2O_9 + H_2O \uparrow \quad (2)$$

XDR measurements were employed to determine the phases developed in the produced bioceramic foams for each case examined (with and without alumina addition). Figure 3 illustrates the XRD spectra of the produced bioceramic foams sintered at 1250 °C for 4 h. The initial HAp powder used is also reported for reasons of comparison. The

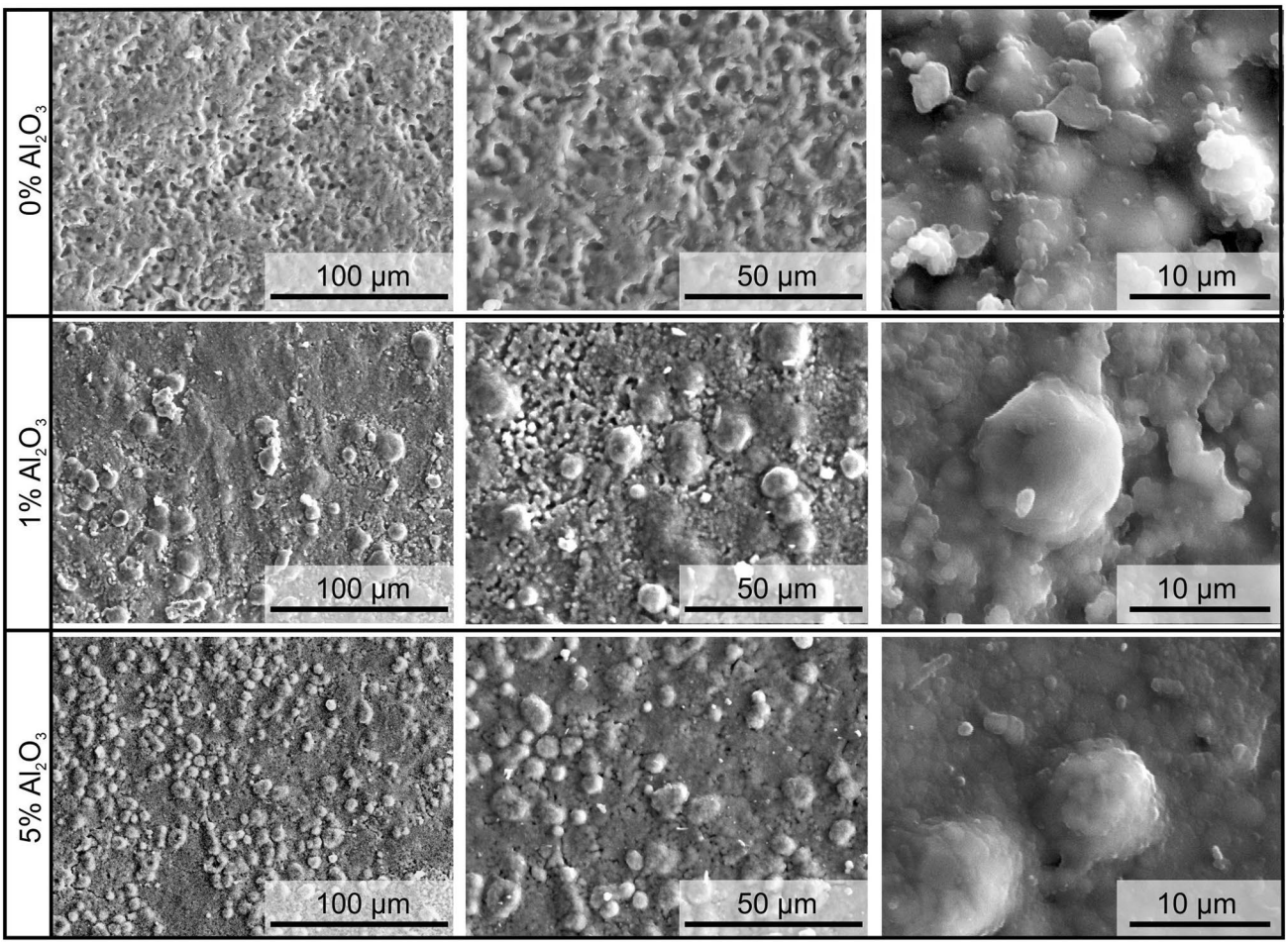

Fig. 2 SEM images of the produced calcium phosphate foam sintered at 1250 °C for 4 h (porosity 65%, mean pore size 0.5 mm) having different alumina additions

XRD pattern of the initial HAp powder presents characteristic peaks of calcium phosphate phases. The XRD pattern from all sintered foams, irrespective of alumina addition, reveals the major presence of HAp, along with the phase of TCP. The phase of CaO was not detected in the pure calcium phosphate foam. In the contrary, the dominant phases are TCP and HAp which can be considered as a BCP composite. Therefore it is safe to deduce that the reaction (1) is more probable to take place. The decomposition of HAp powder during sintering is well documented to occur through dehydroxylation (removal of OH-ion) [21, 22]. Therefore, it is safe to assume that the sintering of the HAp foams leads to partial conversion of HAp into TCP phase. It should be mentioned that failure to detect tetracalcium phosphate (TTCP) could be ascribed to overlapping with the Hap peaks. General spectra obtained from EDX analysis at several regions of the sample dictated that the produced calcium phosphate foam is calcium deficient since the atomic ratio Ca/P is found equivalent to 1.52.

When alumina is added to the HAp powder it leads to a grain refinement. The grains retain their equiaxed geometry but they are significantly smaller (Fig. 2). Moreover a reduction in microporosity is observed. In this case another reaction is assumed to take place. It is proposed in literature that the decomposition of HA, which is in contact with alumina occurs with the formation of Al-rich calcium aluminates according to the reaction [2, 5]

$$Ca_{10}(PO_4)_6(OH)_2 + 6Al_2O_3 \rightarrow 3Ca_3(PO_4)_2 + CaO \cdot 6\,Al_2O_3 + CaAl_2O_4 + H_2O\uparrow \quad (1)$$

In the XRD patterns alumina peaks were detected for composite calcium phosphate foam having 5 wt% alumina addition. Nevertheless, new peaks were also detected in the composite (with alumina addition) calcium phosphate foam, referred as a fourth phase. The fact that these new peaks appeared in the XRD pattern denotes that the fourth phase in the XRD pattern derived from the reaction of alumina with HAp. However, it was not possible to

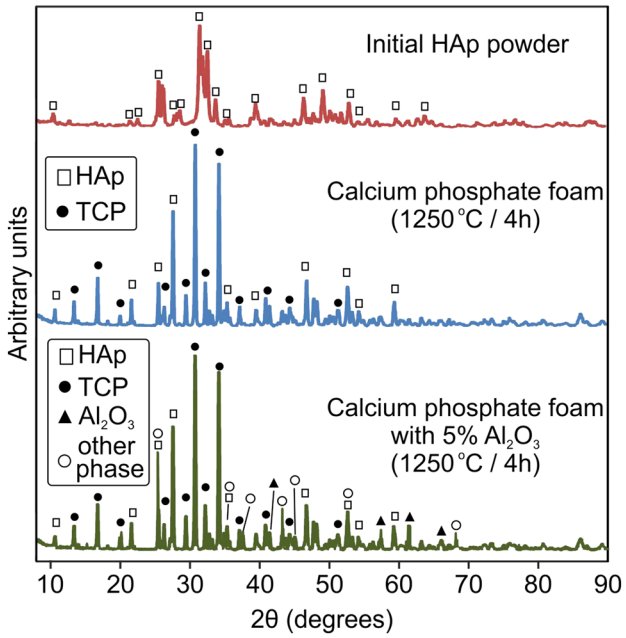

Fig. 3 X-ray diffraction patterns of HAp starting powder and calcium phosphate foams (with and without alumina addition) sintered at 1250 °C for 4 h

characterize this new phase due to severe overlapping of peeks which resulted in ambiguous interpretation of the XRD study regarding this fourth phase.

The reaction of alumina can occur by two diffusion-dependent phenomena, e.g. either Al^{3+} can diffuse into the HAp or Ca^{2+} can diffuse from the HAp into the alumina (Fig. 4). As the reaction proceeds and forms TCP, the HAp becomes Ca-deficient. It is documented that sintering temperatures above 1200 °C favor the formation of both TCP as well as aluminum-rich calcium aluminates [3, 4]. This is also confirmed in this study.

Concerning the pore size distribution and the pore morphological and geometrical characteristics image analysis was performed to several cross-section of each case of produced bioceramic foams. In Fig. 5 the pore size and distribution is shown for all examined bioceramic foam. The pore size and shape resembled the sugar particle characteristics, taking into account the significant decrease in pore sizes due to the sintering shrinkage.

The calcium phosphate foam produced using sugar particles in the range of 0.5–1 mm resulted in pore sizes with a mean value of 0.5 mm. More specifically the pore size was ranging from 0.2 to 0.8 mm, accounting for 90% of the total pores (Fig. 5). Statistical analysis of the pore size revealed that the size distribution of created pores is even more narrow then using sugar particles ranging from 0.25 to 0.5 mm. More specifically the mean pore size was 0.28 mm with the pore size ranging from 0.2 to 0.5 mm accounting for 88% of the total pores. The addition of alumina resulted in a slight sift of the pore size towards higher mean pore size values. However, the pore size distribution maintained its regularity and shape.

The porosity of the produced bioceramic foam can be tailored by simple adjusting the amount of sugar particles. By choosing sugar particles with different particle size ranges it is possible to acquire a purposely tailored porosity and pore size distribution in the produced bioceramic foam.

3.2 Biodegradation/dissolution studies

The weight loss was acquired after normalizing the individual sample's weight prior the immersion in the Tris-HCl buffer solution. The weight loss was determined for the calcium phosphate foam during the 14 days of the degradation assays. The weight loss demonstrated a constant increment with the duration of the immersion period, which implies a steady dissolution (Fig. 6a).

However the addition of alumina resulted in a delay of the dissolution rate of the bioceramic foam. The same amount of weight loss was found after 14 days for the calcium phosphate foam with 5 wt% alumina addition. The same trend is observed in the pH measurements.

It is well reported that TCP presents a high solubility in simulated body fluids. In contrast, the resorption rate for HAp is much lower as compared to TCP and therefore, the HAp dissolves very slowly [1, 19, 20]. This prolonged disintegration time may decelerate the growth of new bone (in

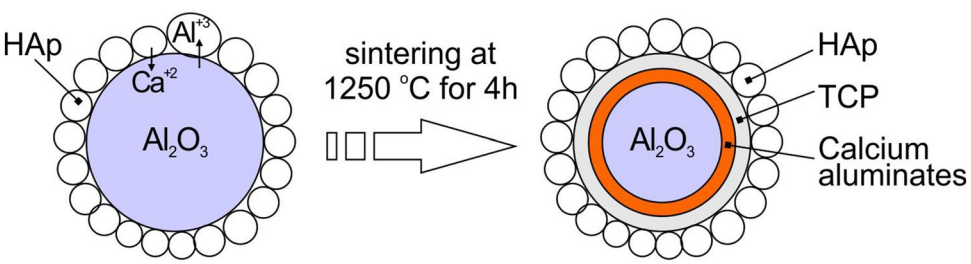

Fig. 4 Schematic representation showing the reaction between HAp and alumina by the diffusion of Ca^{2+} and Al^{+3} ions

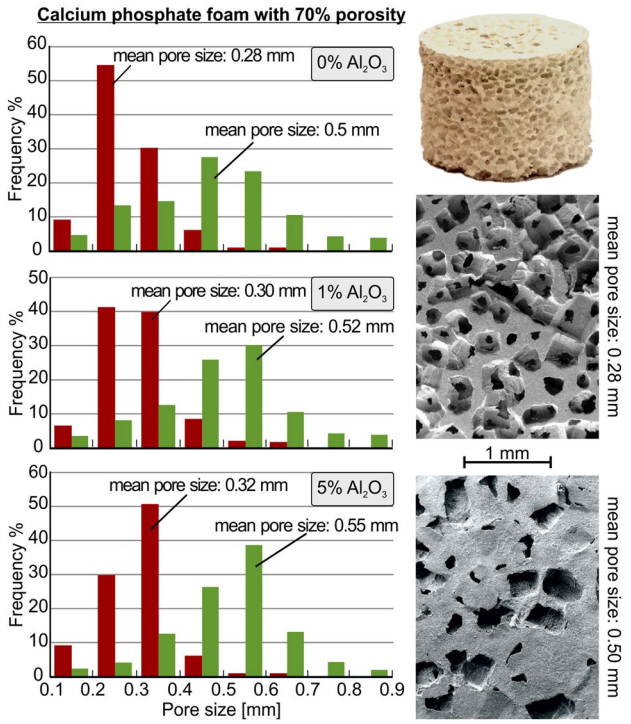

Fig. 5 Pore size distributions versus alumina addition in the porous calcium phosphate sintered at 1250 °C for 4 h

from of apatite) and therefore, constrains the utilization of single phase HAp in implant bone-replacements.

In all produced bioceramic foams characteristic peaks of TCP phase were found by X-ray diffraction. Therefore, it can be presumed that in all examined biorecamic foams that were soaked into Tris-HCl buffer, two processes were simultaneously taking place, the precipitation of new apatite and the disintegration of the TCP phase of the bioceramic foam.

This possible presumption is ascertained by the SEM images of the foam samples depicting the microstructural features developed after soaking in Tris-HCl buffer at different time intervals. For the pure calcium phosphate foam two different morphological microstructures were confirmed from SEM images. It was found that they were regions where deposition of flake-like morphology crystals occurred as well as regions which presented formation of cavities-micropores (Fig. 7).

Because the quantity of the precipitated material was very low, it was not possible to confirm by XRD analysis its crystal structure. Nevertheless, the flake-like morphology of the precipitating phase on the surface resembles the apatite form found in bones and indicates enhanced bioactivity of the foam. It was safely deduced that the interaction between Ca^{+2} and $PO4^{-3}$ ions both derived from the dissolution of the TCP phase ($Ca_3(PO)_4$) resulted in the deposition of flake-like crystals of bone-like apatite in the calcium phosphate foam [18, 23].

The pH measurements also verify this interaction of TCP phase to from apatite via hydrolysis of the TCP phase (Fig. 6b). Thus, the solubility of a TCP surface approaches the solubility of HAp and decreases the pH of the solution. However, for the pure calcium phosphate foam there is a small pH increase after 7 days soaking in Tris-HCl buffer. This slight pH rise is attributed to an inhibition of hydrolysis of TCP phase. The reasons for this inhibition are not yet clarified. However other studies have shown a slight lowering of Ca^{+} when porous TCP is immersed in biological solution at the same time duration (e.g. around 7 days) [16]. This phenomenon is also apparent to the composite bioceramic foam (with 5 wt% alumina addition). However, it was observed after 9-10 days soaking in the Tris-HCl buffer.

The SEM images of the calcium phosphate foams with 5 wt% alumina addition after 9 and 14 days of soaking in the Tris-HCl buffer are also shown in Fig. 7. The same phenophena, as in pure calcium phosphate foam (no alumina addition), were observed, e.g. regions with cavity formation and regions with precipitate deposition. However, in this case the calcium-phosphate minerals precipitates appear as hemispherical globules on the foam surfaces.

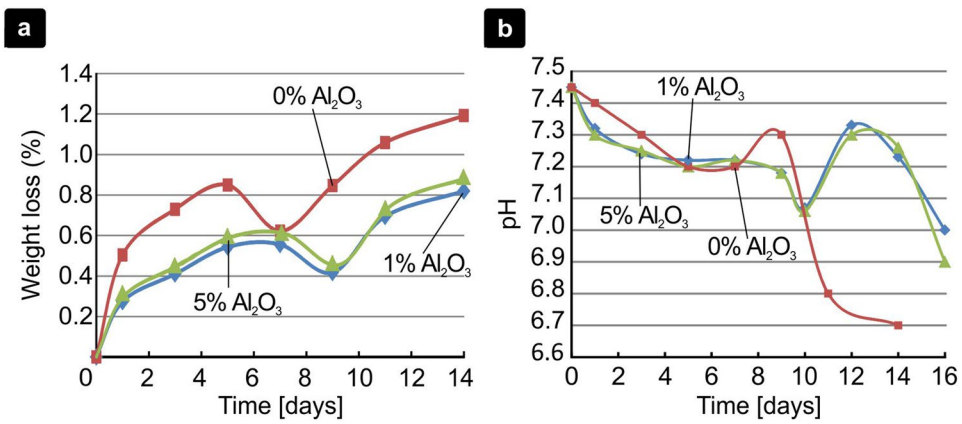

Fig. 6 **a** Weight profile and **b** pH profile of the bioceramics foam having 65% porosity and mean pore size of 0.5 mm after different days of immersion in Tris-HCl solution

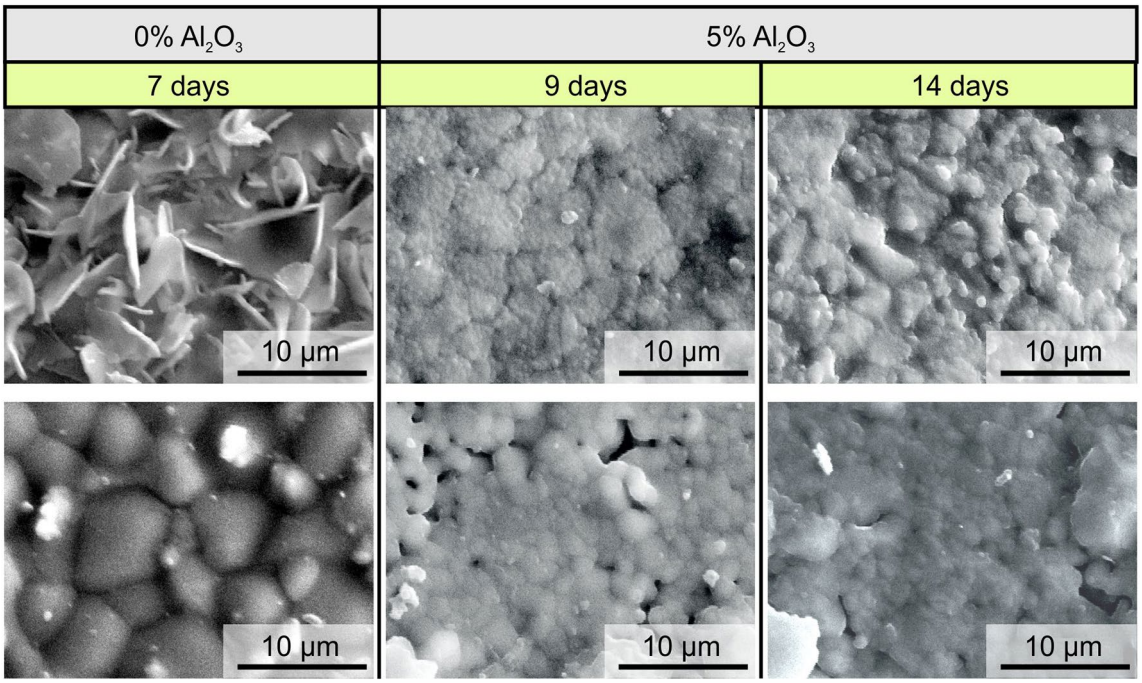

Fig. 7 SEM images of pure calcium phosphate foam (0% Al_2O_3) after 7 days immersion in Tris-HCl buffer solution and SEM images of calcium phosphate foams with 5 wt% alumina addition after 9 and 14 days immersion in Tris-HCl buffer solution. All samples had a 65% porosity and 0.5 mm mean pore size

These morphologies are similar to those reported in other studies [24] characterized as apatite globules. The addition of alumina in the HAp powder mixture resulted in different morphology of the deposited apatite under the same soaking condition. In this case there was absence of petal-like morphologies of deposited apatite indicating the importance of the surface microstructure in the nucleation process of apatite at initial soaking time. After immersion for 14 days, the initial apatite precipitation (in globule morphology) nucleated and increase in crystal size, thus forming larger clusters of apatite that covered the foam surface completely in some regions (Fig. 7). The formation of the different apatite morphologies with respect to the microstructure of the bioceramic foam is schematically shown in Fig. 8.

It should be mentioned that local build-up of solutes may have taken place because all measurements were conducted under static fluid conditions. This means that during the whole duration of the experiment the test solution was not replenished with fresh solution. As a consequence, a change in the initial composition of the solution might have occurred. However, this approximation was followed so as to ensure that no other variables are introduced into the experiment. Nevertheless, these assays may reveal the underlying early-stage reactions of a reinforced (with alumina) calcium phosphate foam implant in reference to the microstructure and phases acquired.

3.3 Mechanical properties

The design of scaffolds for clinical applications requires implants that possess similar porous structure and comparative mechanical strength [1]. Figure 9 shows the variation of compressive stress and elastic modulus with

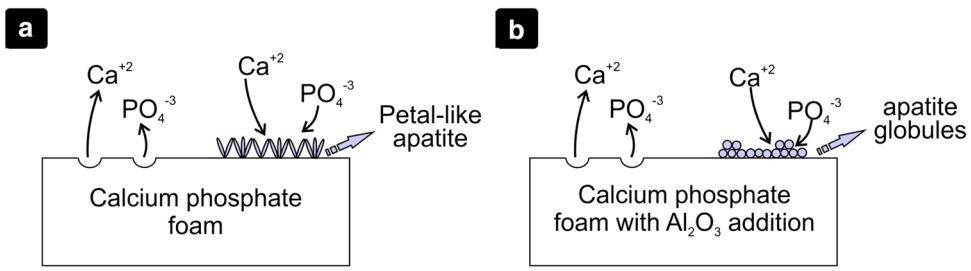

Fig. 8 Schematic representation showing the apatite formation on **a** pure calcium phosphate foam and **b** calcium phosphate foam with alumina addition

respect to porosity and alumina addition to the calcium phosphate foams. The compressive strength of the produced bioceramic foams decreases when the porosity raises, a behavior characteristic for all porous materials. The addition of 1 wt% alumina did not led to any significant alteration of the compression strength of the foam. However, the addition of 5 wt% alumina led to an considerable increase of the mechanical strength for a bioceramic foam with 70% porosity. The struts of the foam become thinner when the porosity increases (Fig. 1c). In this case the alumina particles located inside the strut, seem to carry a significant portion of the load in the foams during the compression test. When the porosity is smaller, the struts of the foam are thicker and the alumina particles seem not to contribute to the foam compressive stress. Therefore, we can deduce that the addition of 5 wt% alumina brings about a size effect for higher porosity bioceramic foams, since their compressive stress increases strongly as the structural scale of the foam falls below a certain value (e.g. thickness of the struts of the foam with respect to alumina powder size). In this case, their compressive stress depends not only on the thickness of the struts of the foam (and hence on the foam porosity), but also on the reinforcement process of the matrix material, e.g. modification of HAp powder with alumina powder addition having a mean powder size of 110 μm.

Representative compressive stress–strain curves obtained for the composite calcium phosphate foams

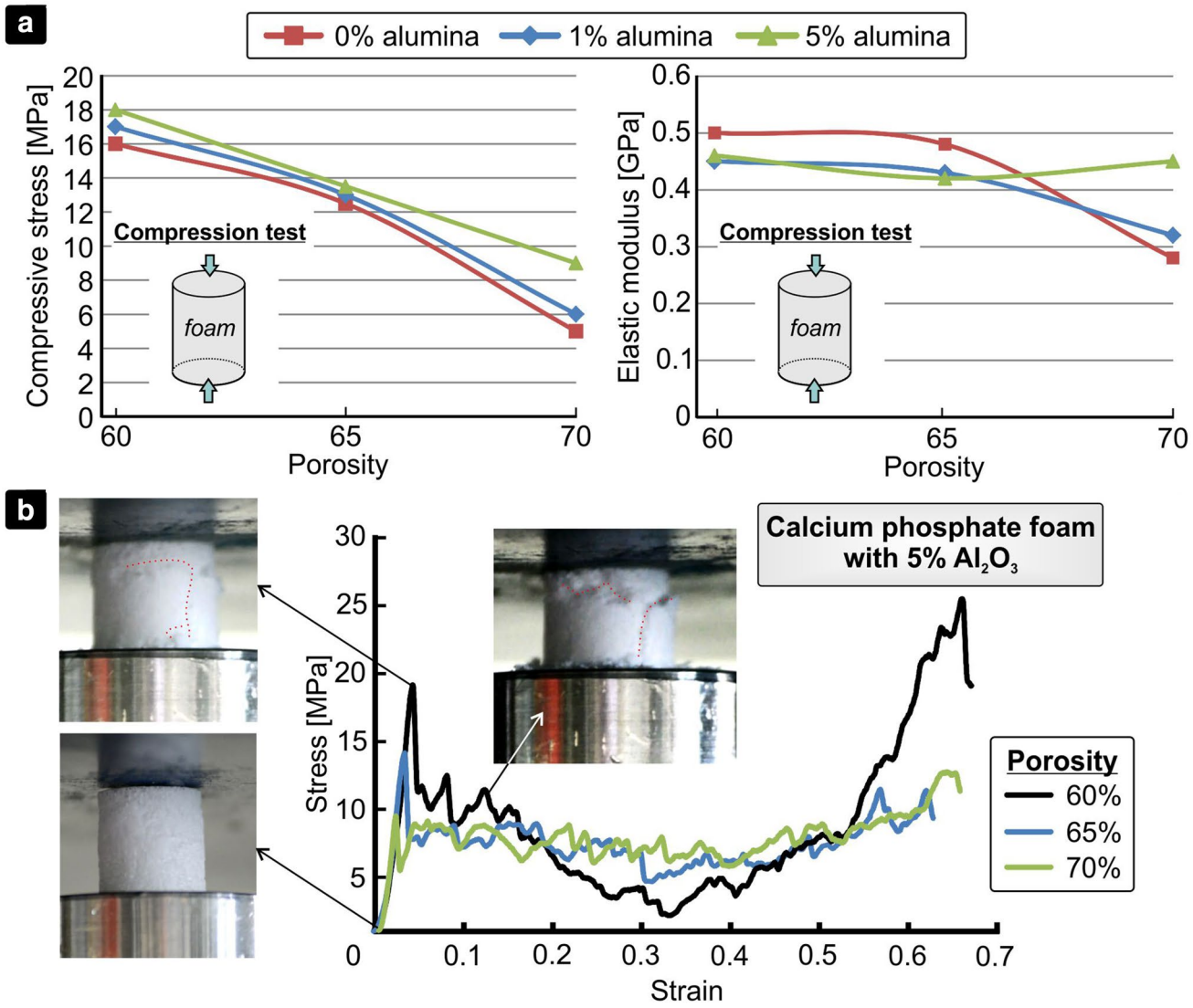

Fig. 9 **a** Compressive strength and elastic modulus of the produced bioceramic foams with respect to porosity. **b** Stress–strain curves of the compressed calcium phosphate foam with 5% w.w. alumina addition, sintered at 1250 °C for 4 h, along with macrographs at different strains. (Cracks: dotted lines)

with 5 wt% alumina addition and several porosities are also given in Fig. 9. The compressive stress–strain curves show a typical behavior of ceramic foams, i.e. subsequent brittle crushing and densification following the fracture.

Regarding the elastic modulus it is clear from Fig. 9 that for porosities of bioceramic foams smaller than 70% the elastic modulus shows no significant dependence on the alumina addition. For porosities above 70% the elastic modulus is increased considerably with a 5 wt% alumina addition. Again, this phenomenon is attributed to size effects between the structural morphology of the struts and the alumina powder mean size.

4 Conclusions

In this study composite calcium phosphate-based foams were fabricated by the addition of small amount of alumina (1 and 5 wt%). A sintering-dissolution technique was employed by using raw cane sugar as a pore former material. The alumina addition resulted in the reduction of micro-porosity of the produced composite bioceramic foams. Moreover, microstructural chances were observed via formation of new phases (calcium aluminates and TCP) that affected both the bio-dissolution rates and the morphological formation of the precipitated apatite on the surface of the foam. The mechanical properties of high porosity (above 70%) composite bioceramic foams were significantly improved by the addition of 5 wt% alumina.

Acknowledgements The authors would like to thank Assoc. Prof. G. Vourlias for helpful comments regarding the XRD analysis. The authors would like to thank Prof. E. Pavlidou for assisting with the SEM characterization.

Compliance with ethical standards

Conflicts of interest The authors have no conflicts of interest to declare.

References

1. Başar B, Tezcaner A, Keskin D, Evis Z (2011) Synthesis, phase transitions and cellular biocompatibility of nanophase alumina–hydroxyapatite composites. Adv Appl Ceram 110:238–243
2. Ji H, Marquis PM (1993) Sintering behavior of hydroxyapatite, reinforced with 20 wt% Al_2O_3. J Mater Sci 28:1941–1945
3. Viswanath B, Ravishankar N (2006) Interfacial reactions in hydroxyapatite/alumina nanocomposites. Scripta Mater 55:863–866
4. Won H, Koh KY-H, Seo S-B, Kim H-E (2003) Properties of fluoridated hydroxyapatite–alumina biological composites densified with addition of CaF_2. Mat Sci Eng C 23:515–521
5. Aminzare M, Eskandari A, Baroonian MH, Berenov A, Razavi Hesabi Z, Taheri M, Sadrnezhaad SK (2013) Review paper-Hydroxyapatite nanocomposites: synthesis, sintering and mechanical properties. Ceram Int 39:2197–2206
6. Jun Y-K, Kim WH, Kweon O-K, Hong S-H (2003) The fabrication and biochemical evaluation of alumina reinforced calcium phosphate porous implants. Biomaterials 24:3731–3739
7. Hannink G, Chris Arts JJ (2011) Bioresorbability, porosity and mechanical strength of bone substitutes: what is optimal for bone regeneration? Injury Int J Care Injured 42:S22–S25
8. Sato M, Tu R, Goyo T, Ueda K, Narushima T (2009) Apatite formation behavior on bio-ceramic films prepared by MOCVD. J Ceram Soc Jpn 117:461–465
9. Ayed FB, Bouaziz J (2008) Sintering of tricalcium phosphate–fluorapatite composites by addition of alumina. Ceram Int 34:1885–1892
10. Lee J-B, Maeng W-Y, Koh Y-H, Kim H-E (2018) Porous calcium phosphate ceramic scaffolds with tailored pore orientations and mechanical properties using lithography-based ceramic 3D printing technique. Materials 11:1711
11. Deng Y, Liu M, Chen X, Wang M, Li X, Xiao Y, Zhang X (2018) Enhanced osteoinductivity of porous biphasic calcium phosphate ceramic beads with high content of strontium-incorporated calcium deficient hydroxyapatite. J Mater Chem B 6:6572–6584
12. Zhang K, Zhang J, Chen K, Hu X, Wang Y, Yang X, Zhang X, Fan Y (2018) In vitro and in vivo assessment of nanostructured porous biphasic calcium phosphate ceramics for promoting osteogenesis in an osteoporotic environment. RSC Adv 8:14646
13. Siqueira L, Guimarães de Paula C, Motisuke M, Gouveia RF, Afonso Camargo SE, Moreira Milhan NV, de Sousa Trichês E (2017) Preparation, characterization and biological studies of B-TCP and B-TCP/Al_2O_3 scaffolds, obtained by gel-casting of foams. Mater Res 20:973–983
14. Ayadi I, Ayed FB (2016) Mechanical optimization of the composite biomaterial based on the tricalcium phosphate, titania and magnesium fluoride. J Mech Behav Biomed 60:568–580. https://doi.org/10.1016/j.jmbbm.2016.03.020
15. Sivaperumal VR, Mani R, Nachiappan MS, Arumugam K (2017) Direct hydrothermal synthesis of hydroxyapatite/alumina nanocomposite. Mater Charact 134:416–421
16. Arifta TI, Munar ML, Tsuru K, Ishikawa K (2017) Fabrication of interconnected porous calcium-deficient hydroxyapatite using the setting reaction of α tricalcium phosphate spherical granules. Ceram Int 43:11149–11155
17. Guidara A, Chaari K, Fakhfakh S, Bouaziz J (2017) The effects of MgO, ZrO_2 and TiO_2 as additives on microstructure and mechanical properties of Al_2O_3-Fap composite. Mater Chem Phys 202:358–368
18. Stergioudi F, Choleridis A, Paulidou E, Smyrnaios E, Michailidis N (2015) Novel production and characterization of porous calcium phosphate suitable for bone tissue engineering applications. Ceram Int 41:3822–3832
19. Yang HY, Thompson I, Yang SF, Chi XP, Evans JRG, Cook RJ (2008) Dissolution characteristics of extrusion freeformed hydroxyapatite–tricalcium phosphate scaffolds. J Mater Sci Mater Med 19:3345–3353
20. Wang Q, Wang Q, Wang J, Zhang X, Yu X, Wan C (2009) Degradation kinetics of calcium polyphosphate bioceramic: an experimental and theoretical study. Mater Res 12:495–501
21. Raynaud S, Champion E, Bernache-Assollant D, Thomas P (2002) Calcium phosphate apatites with variable Ca/P atomic ratio I. Synthesis, characterisation and thermal stability of powder. Biomaterials 23:1065–1072

22. Zhou J, Zhang X, Chen J, Zeng S, De Groot K (1993) High temperature characteristics of synthetic hydroxyapatite. J Mater Sci Mater Med 4:83–85
23. Ahn M-K, Moon Y-W, Koh Y-H, Kim H-E (2013) Production of highly porous triphasic calcium phosphate scaffolds with excellent in vitro bioactivity using vacuum-assisted foaming of ceramic suspension (VFC) technique. Ceram Int 39:5879–5885
24. Bharati S, Sinha MK, Basu D (2005) Hydroxyapatite coating by biomimetic method on titanium alloy using concentrated SBF. Bull Mater Sci 28:617–621